AGU PUBLICATIONS

JGR

Journal of Geophysical Research: Oceans

RESEARCH ARTICLE

10.1002/2017JC012985

Key Points:
- Intense and vertically coherent upwelling and downwelling occur in the Southern Ocean and connect the upper ocean to the abyssal ocean
- Downwelling related to topography in the SO is an overlooked mechanism for fast response of the abyssal ocean to the changing climate
- Residual vertical velocity is primarily determined by the Eulerian component, and related to winds and large-scale topographic features

Correspondence to:
X. Liang,
liang@usf.edu

Citation:
Liang, X., Spall, M., & Wunsch, C. (2017). Global ocean vertical velocity from a dynamically consistent ocean state estimate. *Journal of Geophysical Research: Oceans*, *122*. https://doi.org/10.1002/2017JC012985

Received 12 APR 2017
Accepted 18 SEP 2017
Accepted article online 21 SEP 2017

Global Ocean Vertical Velocity From a Dynamically Consistent Ocean State Estimate

Xinfeng Liang[1], Michael Spall[2], and Carl Wunsch[3,4]

[1]College of Marine Science, University of South Florida, St Petersburg, FL, USA, [2]Physical Oceanography Department, Woods Hole Oceanographic Institution, Woods Hole, MA, USA, [3]Department of Earth, Atmospheric and Planetary Sciences, Massachusetts Institute of Technology, Cambridge, MA, USA, [4]Department of Earth and Planetary Sciences, Harvard University, Cambridge, MA, USA

Abstract Estimates of the global ocean vertical velocities (Eulerian, eddy-induced, and residual) from a dynamically consistent and data-constrained ocean state estimate are presented and analyzed. Conventional patterns of vertical velocity, Ekman pumping, appear in the upper ocean, with topographic dominance at depth. Intense and vertically coherent upwelling and downwelling occur in the Southern Ocean, which are likely due to the interaction of the Antarctic Circumpolar Current and large-scale topographic features and are generally canceled out in the conventional zonally averaged results. These "elevators" at high latitudes connect the upper to the deep and abyssal oceans and working together with isopycnal mixing are likely a mechanism, in addition to the formation of deep and abyssal waters, for fast responses of the deep and abyssal oceans to the changing climate. Also, Eulerian and parameterized eddy-induced components are of opposite signs in numerous regions around the global ocean, particularly in the ocean interior away from surface and bottom. Nevertheless, residual vertical velocity is primarily determined by the Eulerian component, and related to winds and large-scale topographic features. The current estimates of vertical velocities can serve as a useful reference for investigating the vertical exchange of ocean properties and tracers, and its complex spatial structure ultimately permits regional tests of basic oceanographic concepts such as Sverdrup balance and coastal upwelling/downwelling.

1. Introduction

Ocean vertical velocities are both important diagnostics of many different physical processes of the ocean circulation and simplifying descriptive tools. Familiar examples are the role of the vertical velocity, w, in the Stommel-Arons theory (Stommel & Arons, 1960); its role as a uniform vertical velocity in maintaining the "abyssal recipes" balance (Munk, 1966); and the control of Sverdrup balance by the spatial patterns of Ekman pumping (Sverdrup, 1947). Examining the extent to which w in practice has these characteristics not only describes the circulation and diagnoses its controls but also provides useful insights into improving the existing ocean circulation theories. In addition, estimates of w can serve as useful references for estimating and understanding the vertical exchanges of mass, properties, and tracers in the global ocean.

Although its importance has been known for decades, the estimates of w are limited, largely because w that is associated with large-scale ocean circulation is extremely small, of the order of magnitude of 10^{-5} m/s (1 m/d) near the surface and of 10^{-7} m/s (1 cm/d) in the deep ocean, and cannot be measured directly. Many pioneering estimations of w were carried out based on profiles of hydrographic and tracer measurements (e.g., Munk, 1966; Schott & Stommel, 1978; Stommel & Arons, 1960; Wyrtki, 1961) or mooring measurements of horizontal currents (e.g., Wyrtki, 1981), and reached a consensus on the order of magnitude of w in the deep ocean and near the surface. However, these early studies were usually based on simplified vertical exchange or dynamical models and suffered from many caveats. In particular, the spatial and temporal variations of w were commonly ignored and many nowadays well-known processes, such as mesoscale eddies, were not considered.

Recent studies based on numerical models and satellite observations provide updated estimates of w, which usually allow spatial and temporal variations and include the impacts of mesoscale eddies. For instance, Klein et al. (2009) diagnosed w from high-resolution sea surface height data based on the surface quasi-geostrophic method. Their estimates mainly focused on the upper ocean and provided little

information about the deep ocean vertical velocity, which would be significantly different from the values near the surface. General circulation models also routinely provide outputs of vertical velocity from the primitive equations. While w has been considered implicitly when conducting budget analysis of heat, salt, and biogeochemical tracers as well as investigating ocean circulations, such as the Meridional Overturning Circulation (MOC), they are seldom focuses of studies, particularly for the part that is associated with the large-scale circulation.

The purpose of this paper is to briefly describe and interpret the vertical advective flow in the global ocean as determined from an ocean state estimate (e.g., Wunsch & Heimbach, 2013a). As such, it is one of a number of papers (e.g., Liang et al., 2015; Wunsch & Heimbach, 2014) describing the two-decade long global average circulation and its properties such as heat transport. The estimate is both dynamically self-consistent and simultaneously consistent within uncertainty estimates of the various global data sets now available (e.g., Forget et al., 2015a). These features make our estimates different in nature from the outputs of vertical velocity from common general ocean circulation models, in which no observational constraints are usually applied. Also, in contrast to previous studies (e.g., Munk, 1966; Stommel & Arons, 1960), the current study presents not only an estimate of the Eulerian vertical velocity, w_e, which is the vertical velocity in the momentum and continuity equations, but also the component induced by mesoscale eddies, w_b. Here w_b is parameterized following Gent and McWilliams (1990). Note that w_e is the term that is useful in diagnosing the momentum budget, and the sum of w_e and w_b, which will be called the "residual" vertical velocity, w_r, is what matters for the vertical transport of ocean properties and tracers. In this paper, we will mainly provide descriptions of large-scale patterns of three different vertical velocities (w_e, w_b, and w_r), which can serve as references for future studies involving oceanic vertical exchanges. Because the global ocean contains a variety of dynamical regimes, varying with depth and geography, the description can become intricate. The emphasis here is on major features reflecting differing dynamics.

In the following sections, we first describe how the global vertical velocities are reliably estimated in the framework of ECCO (Estimating the Circulation and Climate of the Ocean) in section 2. Then, the 20 year means and standard deviations of the vertical velocities (w_e, w_b, and w_r) are presented in section 3. Zonal averages of vertical velocities as well as the global and basin-wide vertical volume transports are calculated and presented in sections 4 and 5, respectively. At last, section 6 summarizes and discusses the most interesting findings of the global ocean vertical velocities and vertical volume transports.

2. Data and Methods

2.1. The ECCO Estimates

Vertical velocity is part of the ECCO product, a state-of-the-art ocean state estimate. ECCO is directed at estimating the ocean circulation and climate by finding a consistent least squares fit of a general circulation model (MITgcm, Adcroft et al., 2004) to the available global-scale observational data, such as sea level anomaly from altimeters and in situ temperature profiles from Argo (e.g., Wunsch & Heimbach, 2013a). Many ocean processes not included in the simplified models mentioned above are now present. When assimilating observational measurements, Lagrange multipliers enforce the model dynamics and kinematics rather than simply fill in the temporal and spatial gaps based on assumptions or statistical principles. A major advantage of this approach—as compared to what is conventionally called "data assimilation" and used for weather forecasting (e.g., Balmaseda et al., 2013; Dee et al., 2011)—is that the resulting state estimate satisfies the numerical equations of motion for the ocean and conservation laws (e.g., Forget et al., 2015a). More specifically, the estimates are obtained by running the model (MITgcm) freely with adjusted initial, boundary conditions, and internal parameters (e.g., isopycnal, GM, and diapycnal diffusivities). The ECCO estimates can thus be sensibly used to compute heat, vorticity, etc., budgets, not possible with the "jump" solutions used in forecasting (Figure 1 of Stammer et al., 2016). Also, because the estimates are from a free model run and constrained by a large volume of observations, all the variables are both dynamically consistent and close to reality. These characteristics make ECCO estimates suitable for testing existing ocean theories (e.g., Wunsch, 2011), many of which were developed decades ago when only limited observations were available (e.g., Stommel & Arons, 1960).

A number of versions of ECCO state estimates are currently available. Here we use Version 4, Release 1 (v4r1), which is the first global estimate including the Arctic Ocean. In contrast to previous versions, among many advances, control variables in ECCO v4r1 are no longer restricted to the initial conditions and the

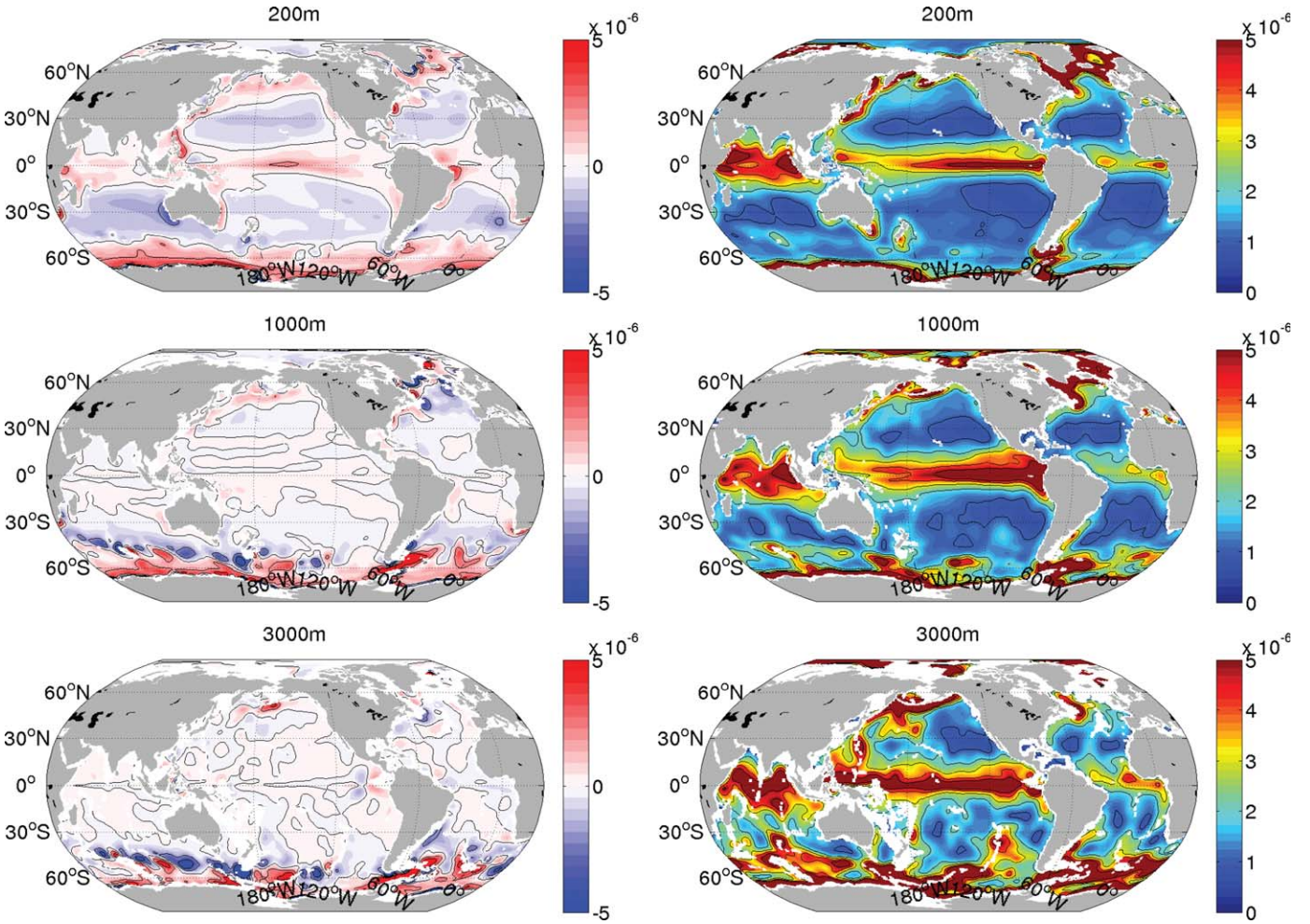

Figure 1. (left column) Twenty-year means and (right column) standard deviations of the Eulerian vertical velocity, w_e. The unit is m/s. The spatial patterns of $\langle w_e \rangle$ vary vertically, from the conventional wind-driven patterns in the upper ocean to topographic related features in the abyssal ocean. Large temporal variations mainly occur at high latitudes, in the tropical regions and near large topographic features in the abyssal ocean.

meteorological forcing, but also include the internal model parameters, such as isopycnal, GM (Gent-McWilliams) and vertical diffusivities. The ECCO v4r1 estimate has 1° zonal resolution and a meridional resolution ranging from about 0.25° near the equator and poles to 1° at midlatitudes. Rescaled height coordinates are used with 50 vertical levels. A priori forcing fields are from the European Centre for Medium Range Weather Forecast (ECMWF) ERA-Interim reanalysis and is corrected through "adjoint" process (Liang & Yu, 2016).

Previous publications have demonstrated that the ECCO v4r1 estimates realistically represent the ocean state. For instance, the estimates fit altimetry (Forget & Ponte, 2015), SST (Buckley et al., 2014), subsurface hydrographic data (Forget et al., 2015a), and the Atlantic Meridional Overturning Circulation (AMOC, Wunsch & Heimbach, 2013b) at or close to the specified noise level. For ocean parameters for which only limited measurements are available (e.g., isopycnal diffusivity, GM diffusivity and diapycnal diffusivity), ECCO v4r1 provides at least physically reasonable estimates (e.g., Forget et al., 2015b). The better agreement between the ECCO v4r1 estimates and observations (e.g., Forget et al., 2015b) as well as the improvements in ocean physics, particularly the vertical diffusivity, shown to compensate the vertical velocity in previous versions of ECCO estimates (e.g., Lu & Stammer, 2004), imply better estimates of the unmeasurable dynamical variables (e.g., vertical velocities) in ECCO v4r1.

2.2. Estimation of Vertical Velocities

In the Eulerian form of the Navier-Stokes equations, the Eulerian vertical velocity, w_e, when combined with the vertical gradients of any property, C, specifically characterizes the advective component of the vertical

movement of C, $w_e\partial C/\partial z$. Describing w_e both in its time-mean and temporal variability is an important subcomponent of the description of any fluid flow. In a turbulent fluid, the time average advection $\langle w_e\partial C/\partial z\rangle$ can be separated into the time averages, $\langle w_e\rangle\langle\partial C/\partial z\rangle$ and a "turbulent" or "eddy" part $\langle w_e'\partial C'/\partial z\rangle$. Here following Danabasoglu et al. (1994), we define an "effective" or "residual" vertical velocity, w_r, that is directly related to the advection of tracers and includes two parts: one is related to the large-scale circulation and is the Eulerian vertical velocity, w_e, and the other is the eddy-induced vertical velocity, w_b. w_b is determined by the activity of mesoscale eddies and acts on the tracer transport. It is an "effective" velocity that has to be derived from indirect measurements. In coarse resolution ocean circulation models, w_b is often parameterized following Gent & McWilliams (1990) and is called the "bolus" vertical velocity (e.g., Danabasoglu et al., 1994).

The Eulerian vertical velocity, w_e, is diagnosed from volume continuity,

$$w_e = -\int_0^z \nabla_h \cdot \mathbf{v_h}\, dz' \tag{1}$$

where ∇_h is the horizontal gradient operator and $\mathbf{v_h}$ is the horizontal Eulerian velocity vector. Note that the total mass change or sea level change over this period contributes to, but has negligible impacts on, the 20 year averaged vertical velocity. Because the direct output of w_e on the grid scale (1°) is noisy, a 3° × 3° smoothing filter (a low-pass spatial filter) was applied to obtain robust large-scale patterns. Smoothing filters using 2° × 2° and 4° × 4° were also tested, and the results are similar.

The eddy-induced vertical velocity, w_b, is parameterized following Danabasoglu et al. (1994):

$$w_b = -\nabla_h \cdot \left(\kappa_{gm}\frac{\nabla_h \rho}{\rho_z}\right) \tag{2}$$

where ρ is potential density, κ_{gm} is the GM (Gent and McWilliams) eddy coefficient, and ∇_h is horizontal gradient operator. Note here κ_{gm} is not obtained through parameterization models but estimated by fitting models to observations. The same 3° × 3° smoothing filter was applied to w_b to obtain large-scale results consistent with w_e.

The vertical transports of properties and tracers are directly related to vertical residual velocity, w_r, which is the sum of w_e and w_b. After obtaining w_e, w_b, and w_r, their 20 year means ($\langle w_e\rangle$, $\langle w_b\rangle$, $\langle w_r\rangle$) and temporal standard deviations (σ_e, σ_b, σ_r) at each grid point are calculated.

3. Estimates of the Global Ocean Vertical Velocities

3.1. Eulerian Vertical Velocity

Twenty-year means of Eulerian vertical velocity, $\langle w_e\rangle$, at three sample depths are presented in Figure 1. In the upper ocean (≈200 m), $\langle w_e\rangle$ shows the conventional wind-driven (Ekman-controlled) patterns, with upwelling (suction) near the equator and downwelling (pumping) in the subtropical ocean basins. Except at the high latitudes and near coastal regions, the strongest upwelling (≈4×10^{-6} m/s) appears in the tropical Pacific Ocean. Note that estimates of $\langle w_e\rangle$ in tropical Pacific at 50 m depth (not shown) are of the order of magnitude of 10^{-5} m/s, consistent with prior estimates that are based on Ekman divergence and geostrophic convergence near the equator (e.g., Qiao & Weisberg, 1997; Wyrtki, 1981). At high latitudes, except in the vicinity of Antarctica and Greenland, where deep and bottom waters are produced, the upper ocean $\langle w_e\rangle$ is dominated by strong upwelling with magnitude up to O(10^{-5}) m/s. Intense upper ocean upwelling also appears in coastal regions, both on the conventionally expected eastern sides, and on the western sides of the ocean basins. A few cases of upwelling on western boundaries have been reported and were usually explained by the interaction between currents and bathymetry (e.g., Aguiar et al., 2014; Roughan & Middleton, 2002). Also, some upwelling occurring over the western boundary can be explained by Ekman pumping (e.g., Qiu & Huang, 1995). In addition, buoyancy-forced flow alone would be expected to result in upwelling along western boundaries and downwelling on eastern boundaries, as found along western Australia, but this effect is likely overwhelmed by the wind-driven upwelling along the eastern subtropical gyres (e.g., Spall, 2003). Detailed analyses of any particular western boundary upwelling need to examine at least the three possible mechanisms mentioned above.

In the ocean interior (≈1,000 m), the spatial structure of $\langle w_e \rangle$ is complex, with a reduction of the direct wind-driven patterns and generally smaller magnitudes ($\sim 10^{-7}$ m/s) except in the high-latitude regions. Away from the lateral boundaries, despite the clear spatial variation, the magnitudes of $\langle w_e \rangle$ are consistent with previous estimates ($\sim 10^{-7}$ m/s) (e.g., Munk, 1966; Munk & Wunsch, 1998). Also, our estimates of $\langle w_e \rangle$ show similar spatial patterns to previous observational and numerical studies (e.g., Cummins et al., 2016; Lu & Stammer, 2004), such as strong downwelling and upwelling on the two sides of the ACC, dominance of downwelling inside major ocean basins, and narrow downwelling bands over equators in the Pacific and Indian Oceans. Disagreements also exist, as expected. For instance, in Lu & Stammer (2004) and the observational part of Cummins et al. (2016), a strong upwelling appears very close to Greenland, but our estimates show a strong downwelling in the same region. Nevertheless, our estimate in that region is consistent with theoretical prediction of Spall and Pickart (2001). They showed that vertical velocity in regions of buoyancy loss should be located close to basin boundaries, because this allows for dissipation to balance the stretching of planetary vorticity caused by the vertical velocity. In addition, bands of upwelling and downwelling appear in the subtropics (e.g., the North Pacific Ocean), and are likely related to the spatial varying isopycnal slopes at the same depth.

On approaching the sea floor, the spatial structure of $\langle w_e \rangle$ in the abyssal ocean is to a large extent related to the bathymetry. Two example regions are noted: (1) $\langle w_e \rangle$ around 3,000 m in the southeastern Pacific shows a feature that is closely related to the East Pacific Rise, with opposite signs on the two sides of the mid-ocean ridge; and (2) along the route of the Antarctic Circumpolar Current (ACC), the bathymetry shoals through Drake Passage. Meanwhile, strong upwelling appears in both Drake Passage and almost the entire Scotia Sea. Also, comparison of $\langle w_e \rangle$ at 1,000 and 3,000 m shows that the strong upwelling and downwelling in the Southern Ocean are vertically coherent. It is likely that the vertically coherent vertical velocities in the Southern Ocean are due to bathymetric control of the equivalent-barotropic currents here, as suggested in previous studies (e.g., de Boer et al., 2013; Marshall, 1995).

As with all process in the ocean, vertical velocity is temporally variable. Figure 1 displays the temporal standard deviations, σ_e, of the Eulerian vertical velocity, associated with variations on all resolved time scales of the 20 year monthly estimates. Large values of σ_e appear in the tropical regions at all depths, consistent with deep-penetrating equatorial waves (e.g., Gill, 1982). High-latitude regions, especially in the vicinities of Greenland and the Antarctic continent, also show strong temporal variations, probably related to deep and bottom water production and export. Large σ_e, but not as large as those at equator and high latitudes, appears at the western boundary currents, particularly the Kuroshio and the Gulf Stream. Furthermore, a clear relationship between the enhanced temporal variations in the abyss and large-scale topographic features appears, suggesting an important role of topography in generating deep ocean variability.

3.2. Eddy-Induced Vertical Velocity

The eddy-induced vertical velocity, or "bolus" vertical velocity, w_b, represents the integral effects of mesoscale eddies on the vertical transport of ocean properties and tracers. Previous studies (e.g., Danabasoglu et al., 1994; Marshall & Radko, 2003) have shown that these components play important roles in various transports in the Southern Ocean. Here we present the estimates of w_b in the global ocean and compare them with the Eulerian component w_e.

Twenty-year means of $\langle w_b \rangle$ are presented in Figure 2. At all the sample depths, the most significant eddy-induced features appear in the Southern Ocean and near Greenland. These structures are associated with steep isopycnal slopes and the expected strong baroclinic instability in those regions. Comparison of $\langle w_b \rangle$ and $\langle w_e \rangle$ at all the sample depths shows a clear compensation between them. For example, the southern Pacific $\langle w_e \rangle$ at 1,000 m shows a band of upwelling extending from the equator southeastward to South America, but for $\langle w_b \rangle$, the same band is downwelling. The compensation tendency of the eddy-induced and the Eulerian transports in the Southern Ocean has been known for a long time, and our estimates show that the compensation is not limited in the Southern Ocean but is a global feature.

Compensation between $\langle w_e \rangle$ and $\langle w_b \rangle$ is also quantified by the term $|\langle w_b \rangle + \langle w_e \rangle| / (|\langle w_b \rangle| + |\langle w_e \rangle|)$. Figure 3 shows the compensation at three sample depths. The smaller the value is, the strong the compensation between $\langle w_e \rangle$ and $\langle w_b \rangle$ is. Generally speaking, the most significant compensation occurs in the ocean interior and away from the surface and the bottom. Compensation between w_e and w_b is common almost

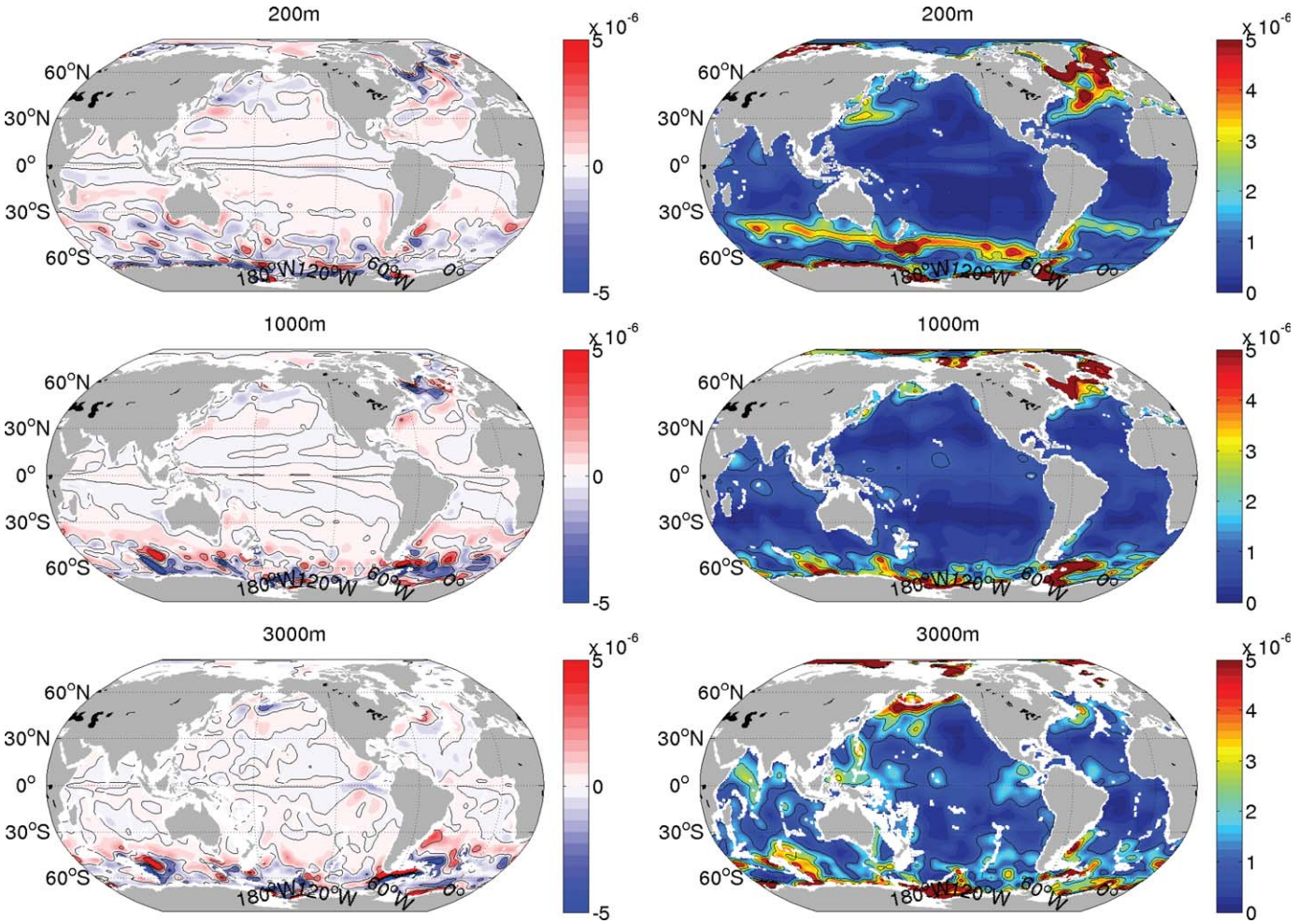

Figure 2. (left column) Twenty-year means and (right column) standard deviations of the eddy-induced vertical velocity, w_b. The unit is m/s. The spatial patterns of $\langle w_b \rangle$ vary vertically. Large temporal variations mainly occur at high latitudes, near strong currents and near large-scale topographic features in the abyss, but not in the tropics.

everywhere, and not confined to the Southern Ocean. This again confirms that the compensation between the Eulerian and eddy-induced transport is more common than previously noticed.

The temporal standard deviations of w_b, σ_b, associated with all resolved temporal variations are presented in Figure 2. σ_b is generally much smaller than σ_e except in a limited number of regions. In particular, in contrast to σ_e, no large values of σ_b appear in the tropical regions, which is likely because the isopycnal slopes associated with equatorial waves are weak (because of proximity to the equator) and because these waves are not a result of baroclinic instability, which is what GM parameterizes. Large σ_b is mainly associated with the major currents in the upper ocean, particularly the Kuroshio, the Gulf Stream and the ACC. High-latitude regions, especially in the vicinities of Greenland and the Antarctic continent, also show strong temporal variations. Enhanced temporal variations in the abyssal ocean are related to the large-scale topographic features.

3.3. Residual Vertical Velocity

The residual vertical velocity, w_r, directly controls the vertical transport of properties and tracers in the ocean. Figure 4 displays the spatial structures of $\langle w_r \rangle$ at three sample depths. Visually, $\langle w_r \rangle$ in the upper ocean is similar to $\langle w_e \rangle$, with strong upwelling in the tropical regions, uniform downwelling in the subtropical ocean basins and enhanced upwelling in the Southern Ocean, indicating that the upper ocean $\langle w_r \rangle$ is dominated by $\langle w_e \rangle$. But, $\langle w_b \rangle$ does have clear impacts on the upper ocean $\langle w_r \rangle$ in some regions. For instance, the spatial patterns of $\langle w_r \rangle$ in the Southern Ocean are not as smooth as those of $\langle w_e \rangle$. Also, the

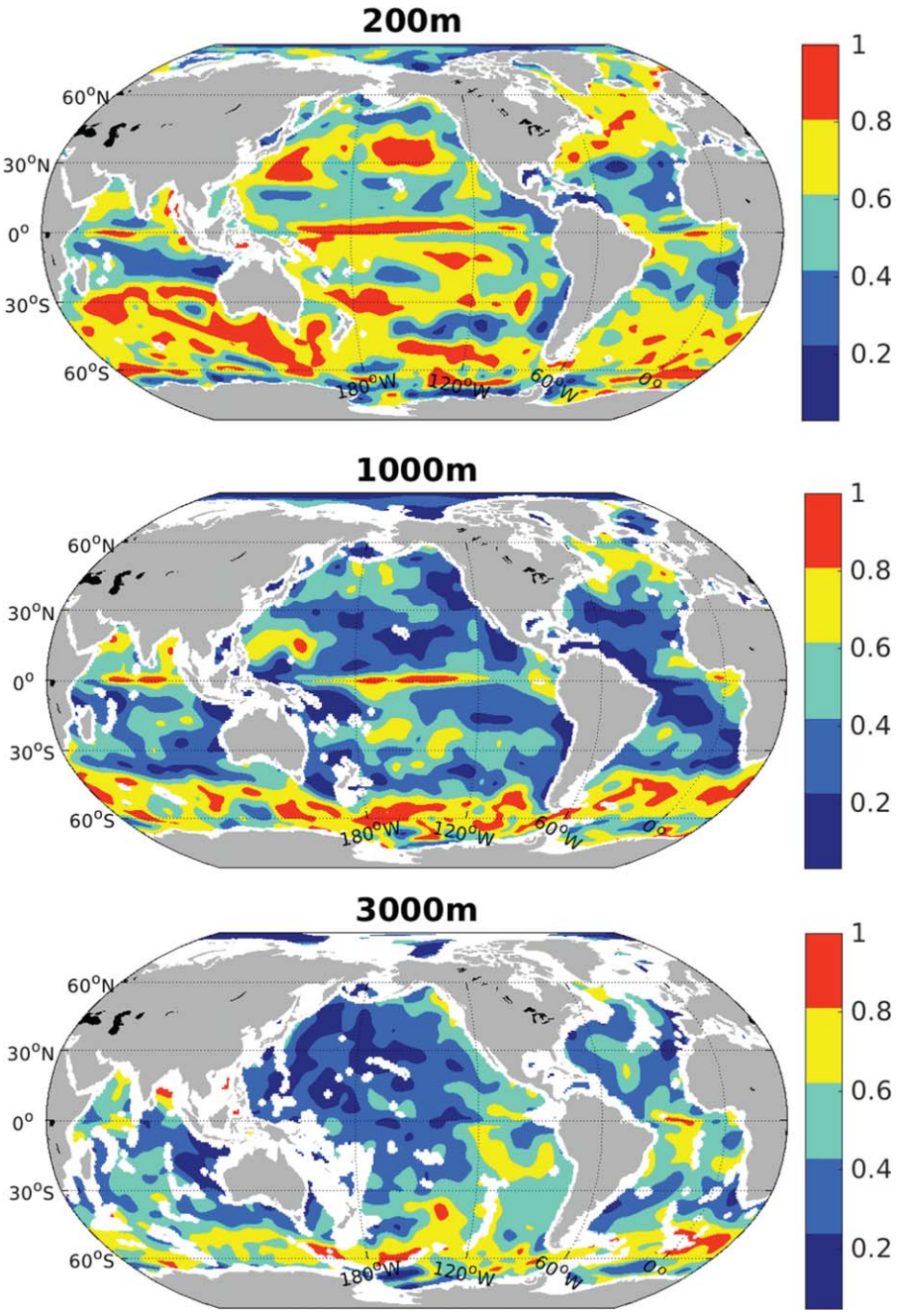

Figure 3. Quantification of the compensation between w_e and w_b, $|\langle w_b\rangle+\langle w_e\rangle|/(|\langle w_b\rangle|+|\langle w_e\rangle|)$ at three sample depths. The smaller the values is, the strong the compensation is. Clearly, the compensation between w_e and w_b is not limited in the Southern Ocean but is a global feature.

upwelling in w_e in the tropical Atlantic is clearly suppressed by w_b. At high latitudes, particularly near Greenland, strong downwelling in $\langle w_r\rangle$ appears.

$\langle w_r\rangle$ in the deep and abyssal oceans generally shows less noisy spatial patterns than do either $\langle w_e\rangle$ or $\langle w_b\rangle$. The strongest residual upwelling and downwelling in the deep and abyssal oceans occur in the Southern Ocean and near Greenland, where their magnitudes reach O(10^{-5}) m/s. $\langle w_r\rangle$ in the deep and abyssal Southern Ocean is more intense and more complicated than in the upper ocean and appears vertically coherent. These features are part of the special nature of the Southern Ocean and could have important implications for the vertical exchange of oceanic properties and tracers. Also, it is likely that the signals of climate change

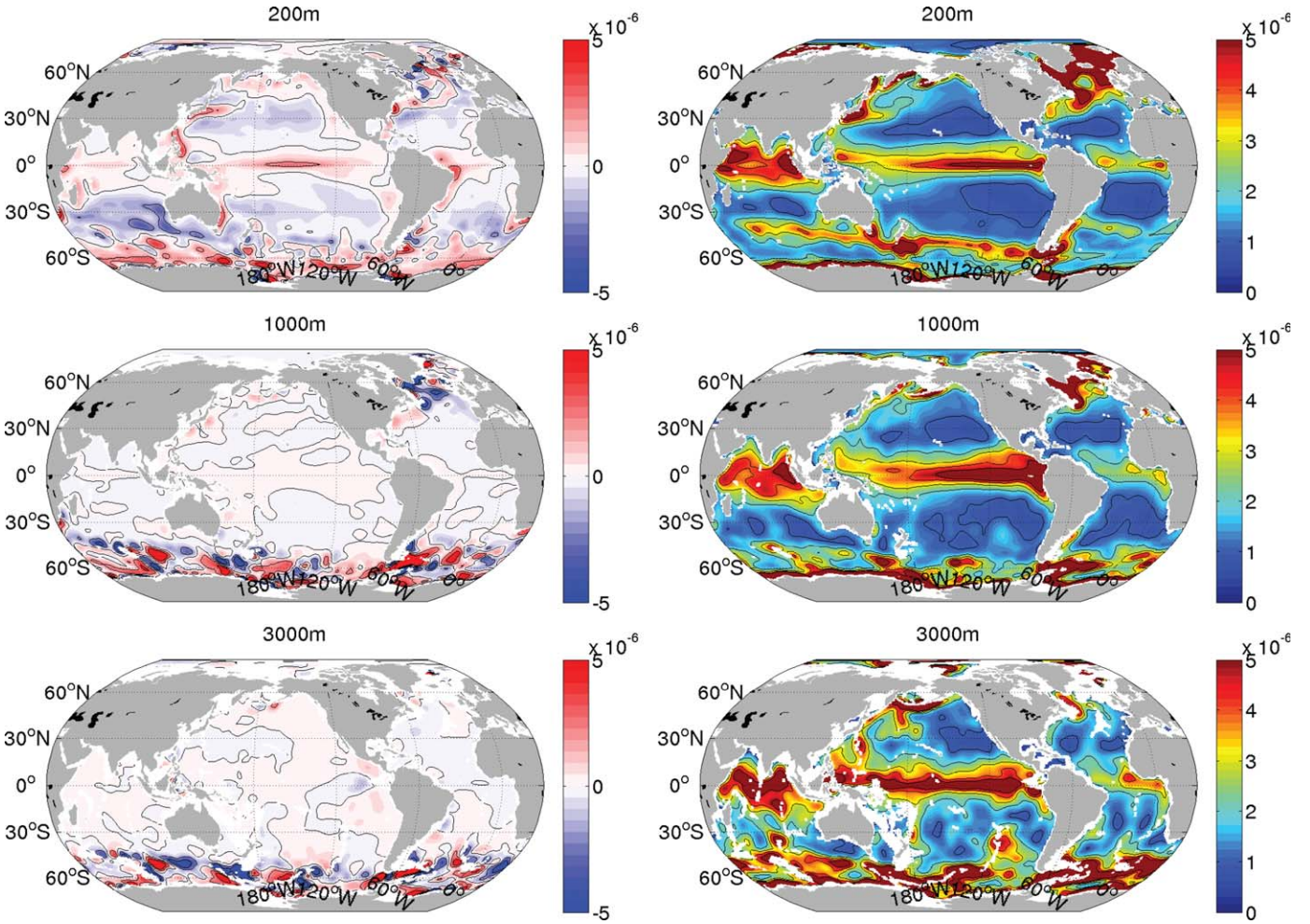

Figure 4. (left column) Twenty-year means and (right column) standard deviations of the residual vertical velocity, w_r. The unit is m/s. Vertically, the Pacific and the Indian change from downwelling dominance around 200 m to upwelling dominance around 3,000 m. The Atlantic shows a dominant downwelling at all these depths. Intense and vertically coherent structures appear in the Southern Ocean. The temporal variation displays a pattern of the combination of σ_e and σ_b.

or anthropogenic impacts (e.g., abnormal temperature, anthropogenic CO_2) that enter the surface ocean can propagate into the deep and abyssal oceans through those regions with vertically coherent downwelling in a much faster pace (~10 years). And this could be one of the reasons why significant warming has been observed in the deep and abyssal Southern Ocean but not as significant in other regions of the global ocean (e.g., Purkey & Johnson, 2010; Wunsch & Heimbach, 2014). Since the vertically coherent structures appear in both upwelling and downwelling, they could not be entirely associated with the deep/abyssal water formation and export. In other words, the movement of water masses may not be the sole mechanism for transferring climate change signals to the deep and abyssal oceans on decadal time scales. The possible roles of the vertically coherent structures in the Southern Ocean in transporting the climate changing signals will be explored in detail in a future study.

The temporal standard deviations of w_r, σ_r are displayed in Figure 4. The spatial distribution of σ_r consists of patches of large values from both σ_e (Figure 1) and σ_b (Figure 2). Specifically, large σ_r appears in the whole water column near the equator, near the major ocean currents, in the vicinities of Greenland and the Antarctic continents, as well as near the large-scale topographic features of the abyssal ocean. Strong temporal variations in the vertical transport of ocean properties and tracers are therefore expected in those regions. Subtropical ocean basins generally show much weaker temporal variations. Note that in contrast to the temporal means, no significant cancelation occurs between w_e and w_b in the temporal variability.

4. Zonal Averages of Vertical Velocities

Vertical movement is a major part of the meridional overturning circulation (MOC), which is usually defined from the zonal integration of the mass transport. Here we present the zonal averages of the vertical velocities in major ocean basins, the Pacific, the Atlantic and the Indian (Figure 5). We also compare the zonal averages with prior studies and discuss the impacts of zonal average in interpreting the dynamics of vertical exchange. Note that because the values of the global vertical velocities span a wide range, structures of small values exist but are not revealed in Figure 5.

4.1. Zonal Averages of W_e

The left column of Figure 5 shows the zonal average of the Eulerian vertical velocity, $\langle\overline{w_e}\rangle$. South of 30°S, $\langle\overline{w_e}\rangle$ in all three ocean basins shows a similar latitudinal structure, that is, intense downwelling with magnitude above 5×10^{-6} m/s in the vicinity of the Antarctic continent, and broad upwelling and downwelling occupying almost the whole water depth extending northward. The broad upwelling and downwelling between 60°S and 30°S is related to the "Deacon cell," whose Eulerian nature has been discussed previously (e.g., Speer et al., 2000).

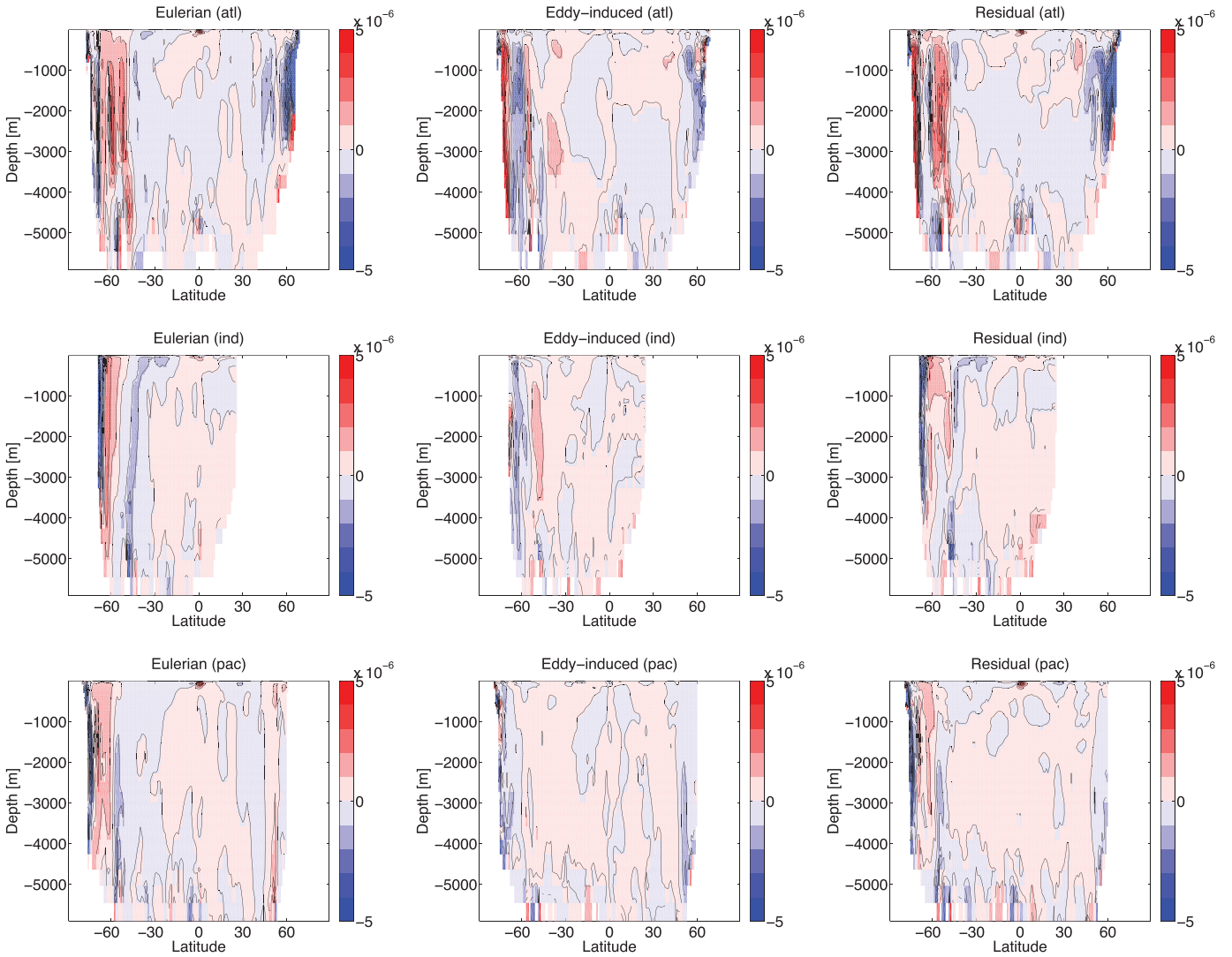

Figure 5. Zonal averages of the 20 year means of vertical velocities (w_e, w_b, and w_r) in the Atlantic (atl), the Pacific (pac), and the Indian (ind); the three columns, from left to right, are estimates of $\langle\overline{w_e}\rangle$, $\langle\overline{w_b}\rangle$, and $\langle\overline{w_r}\rangle$, respectively. The unit is m/s. Conventional features like the "Deacon Cell" are revealed in $\langle\overline{w_e}\rangle$. But, some potentially important features, such as the topography-related intense upwellings and downwellings in the Southern Ocean (e.g., Figure 1), are averaged out.

$\langle\overline{w_e}\rangle$ in the tropical and subtropical regions displays clear differences between the Atlantic, and the Indo-Pacific Oceans. Between 30°S and 30°N, both the Indian and the Pacific show a vertically coherent upwelling that almost extends almost from the seafloor to the surface. But within the same latitude band, the Atlantic displays a more complex pattern. North of 30°N, both the Atlantic and the Pacific show a latitudinal distribution of downwelling-upwelling-downwelling. This pattern is somewhat similar to that in the Southern Ocean. In the northern Atlantic, the magnitude of $\langle\overline{w_e}\rangle$ around 60°N is up to O(10^{-5}) m/s. In the northern Pacific, however, only weak downwelling O(10^{-6}) m/s appears, probably because no deep water is formed there.

Comparing the zonal averages (Figure 5) with the three-dimensional values of w_e (Figure 1) indicates that the conventional two-dimensional or zonally averaged views of ocean circulation hide many dynamics that are important for the vertical transport. For instance, the zonal distribution of upwelling and downwelling in the Southern Ocean as well as its relationship with the zonal change of topography disappear in the zonally averaged view. As a consequence, some possible responses of the vertical transport of heat, salt, or biogeochemical tracers to the changing climate will be missed in those zonally averaged conceptual/numerical models. For instance, a major portion of the vertical velocity in the Southern Ocean is in practice related to the strength of the deep ocean currents and bathymetry rather than directly wind-driven (Ekman Pumping). Thus, in addition to the possible latitudinal wind shift (e.g., Toggweiler et al., 2006), changes in the wind stress magnitudes, which might lead to a changed Circumpolar Circulation, can induce changes in the deep ocean vertical velocity as well. As a consequence, more or less CO_2 can be transported into/out of the deep ocean due to wind intensity changes alone. This plausible mechanism, through which the Southern Ocean can also regulate the atmospheric CO_2, is missed in the two-dimensional views of the ocean circulation.

4.2. Zonal Averages of W_b

Figure 5 also shows the zonal average of the eddy-induced vertical velocity, $\langle\overline{w_b}\rangle$. South of 30°S, in the vicinity of the Antarctic continent large positive values up to 5×10^{-6} m/s appear. Strong downwelling and upwelling extending from seafloor to the surface occur further north. This latitudinal distribution is almost the opposite to that in $\langle\overline{w_e}\rangle$ in the same region, consistent with compensation of eddy-induced and Eulerian transports in the Southern Ocean that is known from earlier studies (e.g., Johnson & Bryden, 1989).

Visually, $\langle\overline{w_b}\rangle$ in the tropical and subtropical regions of all three ocean basins is not as vertically coherent as $\langle\overline{w_b}\rangle$ in the Southern Ocean. In the Atlantic Ocean, $\langle\overline{w_b}\rangle$ shows a clear vertical reversal between 30°S and 30°N, with downwelling in the upper 3,000 m and upwelling below 3,000 m south of the equator. North of the equator, upwelling occurs in the upper 2,000 m and downwelling below 2,000 m. This reversing structure is consistent with reversal of the isopycnal on the two sides of the equator. North of 30°N, both the Atlantic and the Pacific show vertically coherent downwelling. In the North Atlantic, it is especially intense (up to 5×10^{-5} m/s) and does not show the opposing effects to $\langle\overline{w_e}\rangle$, producing an even stronger downward transport than from the Eulerian component alone. Downwelling also appears north of 30°N in the Pacific, but is significantly weaker than that in the Atlantic.

4.3. Zonal Averages of W_r

The zonally averaged residual vertical velocity, $\langle\overline{w_r}\rangle$, is displayed in the right column of Figure 5. Consider first the region south of 30°S. In the Atlantic sector, vertically coherent structures with a latitudinal quadrupole pattern of upwelling-downwelling-upwelling-downwelling occur south of 30°S. Strong upwelling and downwelling in the south end of the Atlantic section occur inside the Weddell Sea (see Figure 4). The intense upwelling between 60°S and 50°S in the Atlantic sector is associated with the strong upwelling in Drake Passage and the Scotia Sea. In the Indian and the Pacific sectors, $\langle\overline{w_r}\rangle$ south of 30°S shows a similar latitudinal structure, that is, downwelling-upwelling-downwelling northward.

North of 30°S in the Atlantic, downwelling occurs in the intermediate layer centered at a depth that increases from about 2,000 m near 30°S to around 3,000 m near 30°N. Patches of upwelling appear in the upper 2,000 m between 30°S and 30°N in the Atlantic, but a large portion of that is due to the extreme values in the western boundary current (see Figure 4). Within the same latitude band, the Indian and the Pacific are clearly dominated by upwelling. These features indicate that water masses rise vertically in the tropical and subtropical regions of the Indian and Pacific Ocean. North of 30°N, the Atlantic shows strong downward $\langle\overline{w_r}\rangle$ with magnitude up to O(10^{-5} m/s). The Pacific Ocean also shows downward $\langle\overline{w_r}\rangle$ in the

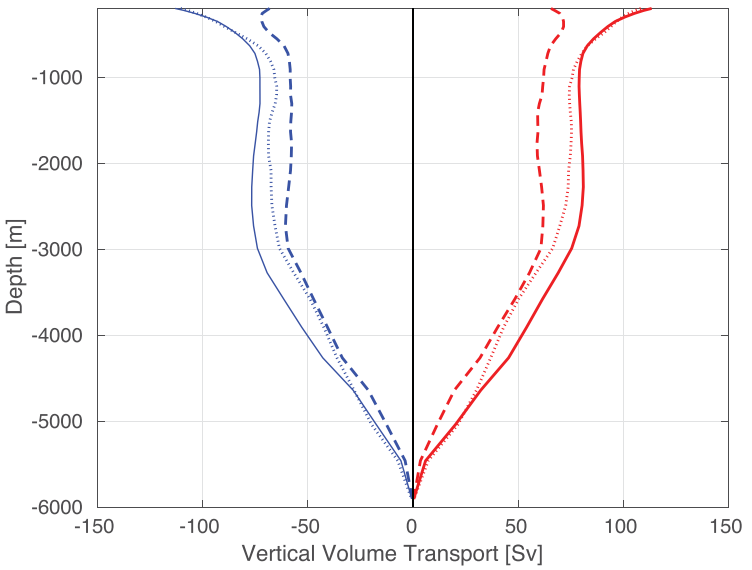

Figure 6. Global integrals of the upward (red) and of the downward (blue) volume transports and their sums (black). The Eulerian, eddy-induced and residual vertical transports are shown as solid, dash and dotted lines, respectively. Note the sums of the integrals of positive (negative) w_e and w_b are not equal to the integrals of the positive (negative) w_r.

same latitude band, which is much weaker than that in the Atlantic, as expected from the latitudinal distributions of $\langle\overline{w_e}\rangle$ and $\langle\overline{w_b}\rangle$.

5. Vertical Volume Transport

The global integrals of upward and of downward transports from w_e, w_b, and w_r at each depth are presented in Figure 6. w_e and w_b are estimated independently and separately satisfy mass continuity. The area integrals for each of w_e, w_b, and w_r are zero at all the depths, obeying a basic consistency check. Between 500 and 3,000 m, the magnitude of the Eulerian upward or downward transports reaches 75 Sv and magnitudes of the eddy-induced values are around 60 Sv. Meanwhile, the residual upward and downward transports are around 70 Sv. Note that because at the same location, w_e and w_b are not necessarily of the same sign, the sums of the integrals of positive (negative) w_e and w_b are not equal to the integrals of the positive (negative) w_r. The large residual vertical volume transport in the intermediate layer is related to ocean vertical exchange of heat, salt, nutrient, and other biogeochemical tracers. Note that these values are obtained after applying the $3^\circ \times 3^\circ$ smoothing filter; unsmoothed values are larger.

The vertical structure of the residual volume transport, W_r, which includes both the upward and downward components, in four major ocean basins is calculated and compared with existing estimates (Figure 7). W_r shows significant differences among the major ocean basins. In the Southern Ocean, upward W_r occurs from 300 m to about 2,500 m, with a maximum value of 12 Sv at about 1,000 m, and downward W_r occurs below about 2,500 m, with a maximum value of 16 Sv at about 3,800 m. The Pacific is dominated by positive W_r over the whole water depth, with a large value of 10 Sv appearing between 3,000 and 4,000 m. The Indian Ocean, except in the depth range between 300 and 1,000 m, also shows upward W_r and below 2,000 m magnitudes of about half of the Pacific transport at the same depth. The Atlantic is the only basin showing a dominance of downward W_r in the upper 3,500 m, with a maximum value of 14 Sv at around 1,400 m.

As revealed in previous studies (e.g., Liang et al., 2015; Marshall & Speer, 2012), the Southern Ocean is particularly important in the exchange of heat, carbon and other tracers between the upper and deep oceans. Here W in the Southern Ocean is further partitioned into three sectors within the Atlantic, Indian and Pacific Oceans (Figure 7). South of 30°S, the Atlantic sector shows a clear upward W_r above 4,000 m, with a large value around 11 Sv between 1,400 and 2,100 m. Below 4,000 m, W_r in the Atlantic sector is close to zero. In contrast, both the Pacific and the Indian sectors south of 30°S show a "sandwich" structure, with downward transport in the upper ocean, upward transport in the middle layer, and downward transport in the deep and abyssal ocean. W_e in the different sectors of the Southern Ocean shows similar patterns to W_r, except that the upward transport in the middle of the water column in the Pacific and the Indian sectors is limited. W_b in all the three sectors is much smaller than W_e. Also, W_b shows patterns in the Atlantic sector distinct from the Pacific and Indian ones, namely, being mainly downward in the Atlantic sector, but upward in much of the Pacific and Indian sectors.

The basin-wide integrals of W_r can be compared with previous ocean circulation schematics (e.g., Talley, 2013). North of 30°S, the result in the Pacific Ocean is generally consistent with existing descriptions of the global overturning circulation (e.g., Figure 4 in Talley, 2013), with a dominance of upward transport. However, in the Atlantic Ocean, the downward transport not only appears in limited regions at high latitudes as shown in the previous schematics but also over the major portion of the ocean basin (see Figure 4). In the Indian Ocean, even though the upward transport that is marked in Talley's schematic (Talley, 2013) appears above 300 m and below about 1,100 m, the depth range between 300 and 1,100 m is dominated by a downward transport, the opposite to her schematic of the MOC. In the sectors south of 30°S, net sinking of water mainly occurs in water column below about 1,000 m in the Pacific sector and below 2,000 m in the

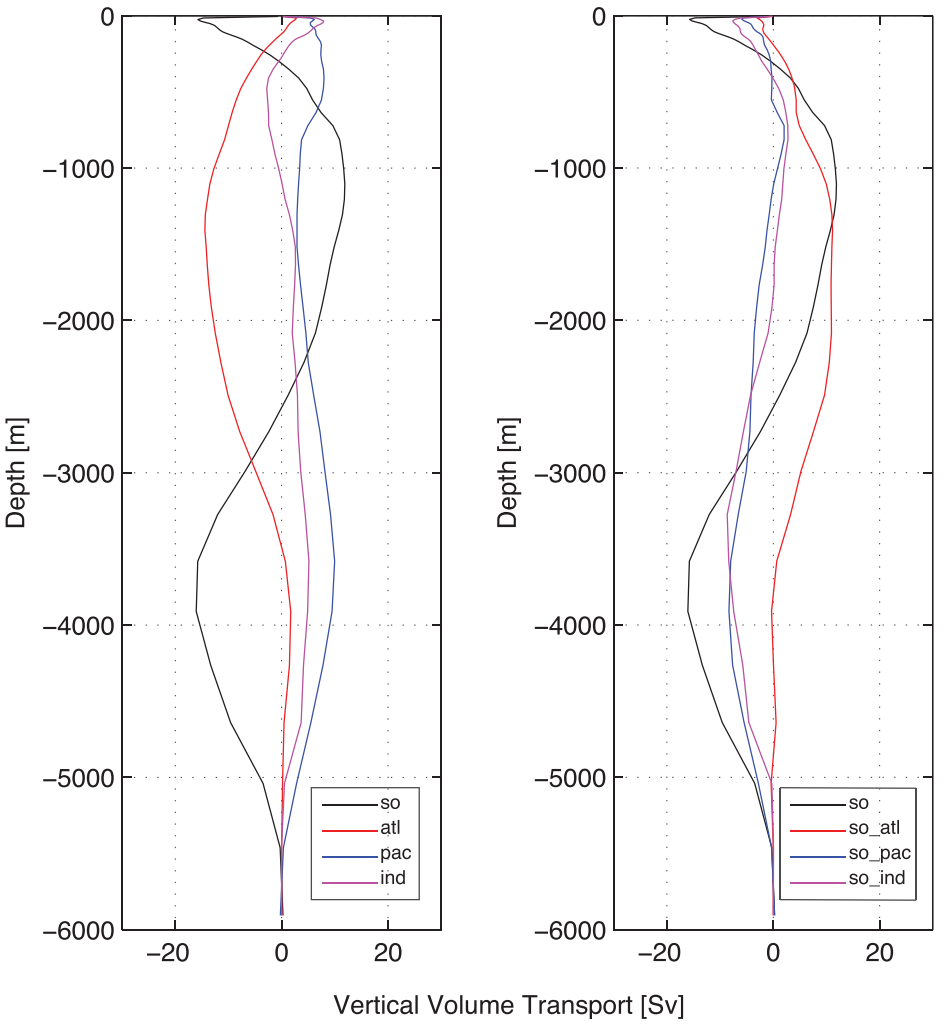

Figure 7. Vertical volume transport, W_r, from ECCO v4r1. (left) Basin-wide integrated vertical volume transport in four ocean basins. Here the ocean basins are defined as the Pacific (>30°S), the Atlantic (>30°S), the Indian (>30°S) and the Southern Ocean (<30°S). (right) Partition of the vertical volume transport in the Southern Ocean. Here the Southern Ocean is further divided into three sectors: the Pacific sector (<30°S), the Atlantic sector (<30°S) and the Indian sector (<30°S).

Indian one. The Atlantic sector, on the other hand, is dominated by a net upward transport in the whole water depth. The reasons for these differences from previous descriptions (e.g., Talley, 2013) must lie with the use here of a much more diverse data set than has generally been employed, with the imposition of oceanic dynamics and the full-meteorological forcing fields, and the ability to compute a uniform time average over 20 years.

6. Summary and Discussion

A first step is taken to describe and understand the global ocean vertical advective exchanges from a dynamically consistent and data-constrained ocean state estimate ECCO v4r1. Three elements of the vertical velocity are described. Due to the various dynamical regimes in the global ocean, the description is intricate and a thorough discussion is impossible in a comparatively short space and only a brief summary of major results is attempted here.

Estimates of the global ocean vertical velocities from ECCO v4r1 show many well-known features, including Ekman-suction upwelling in the tropical upper ocean, downwelling in the subtropical upper ocean, and the Eulerian Deacon cell as well as the compensation between the eddy-induced and Eulerian transport in the

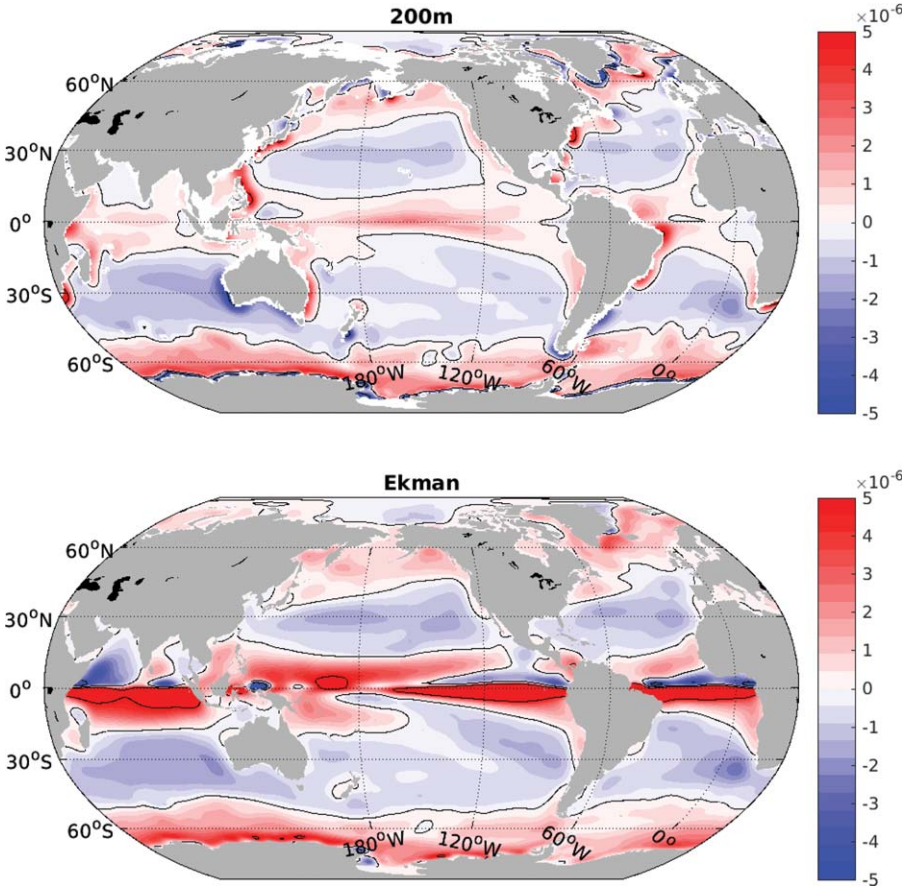

Figure 8. Dominance of w_e near the surface. Upper: w_e in m/s near the surface; Lower: the Ekman pumping calculated with wind stress curl from ECCO v4r1. Comparison of the w_e near surface and the Ekman pumping indicates that w_e near surface is largely determined by the wind stress curl.

Southern Ocean. The vertical volume transport in the major ocean basins is generally consistent with existing descriptions of the global overturning circulation.

A number of new results also appear, including the intense, vertically coherent structures in the North Atlantic and the Southern Ocean, representing strong vertical advective exchanges between upper and lower oceans of heat, salt, carbon, and other tracers. These "pipes" connect the atmosphere and the upper ocean to the deep and abyssal oceans and seems to be a mechanism, in addition to the wind-driven upwelling and the formation of deep and bottom waters, for fast (on the time scale of decades) response of the deep and abyssal oceans to the changing surface climate. Note that these "pipe-like" structures are likely related to the upward/downward slopes that are similar at every depth and are the consequences of barotropic currents flowing over bathymetry. Following any particular water mass, these structures will not necessary move the water mass vertically over the bathymetry. However, these structures could still potentially affect the vertical transport of properties of water masses and tracers. The major reason is that in addition to the advective movements of water mass along isopycnals, other processes, particularly the isopycnal mixing, could spread the properties (e.g., temperature, salinity) and tracers within the isopycnal layer (but at different depths) as the water mass moves over bathymetry. As a consequence, these bathymetry-related structures at high latitudes may act like "elevators" for tracers and properties and produce a net effect on their vertical transports over the bathymetry. Detailed analyses involving both the advective and diffusive processes will be conducted to further explore the potential impacts of those "pipe-like" structures to the vertical exchanges of oceanic properties and tracers.

The residual vertical velocity, which is responsible for the vertical transport of properties and tracers, is the sum of the Eulerian and the eddy-induced components. Previous studies showed that the eddy-induced

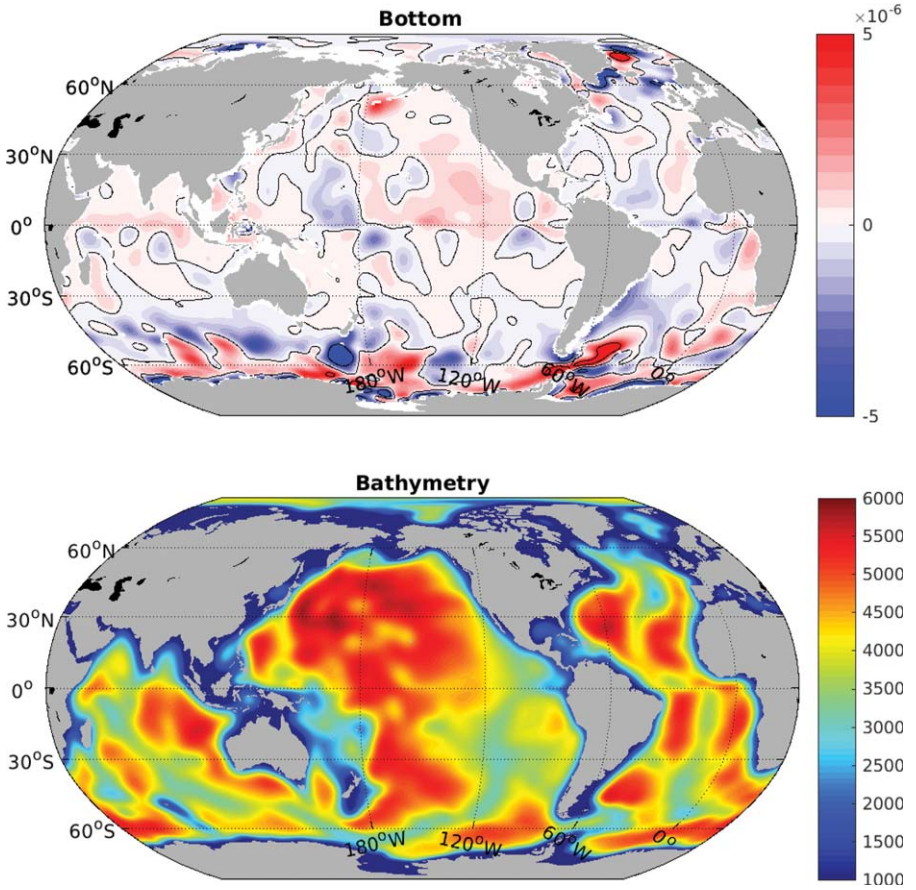

Figure 9. Dominance of w_e near the bottom. (top) w_e in m/s near the bottom; (bottom) the large-scale (smoothed) topography. Examining the relationships between w_e near the bottom and the large-scale bathymetry shows that the bottom w_e is primarily determined by the interaction between the bottom currents and bathymetry.

transport offsets the Eulerian transport in the Southern Ocean, resulting in the suppression of transport by the Deacon cell (e.g., Danabasoglu et al., 1994). Estimates here show that the compensation between w_e and w_b occurs not only in the Southern Ocean but over much of the global ocean with the Eulerian transport tending to dominate.

Spatial patterns of w_e indicate different physics operating at different depths. The upper ocean is controlled by Ekman pumping and suction (Figure 8), but in the deep ocean, topographic controls are dominant (Figure 9). Figure 10 shows the correlations between w_e in the ocean interior and the surface w_e as well as the w_e near the seafloor. The results indicate that globally the wind-driven patterns can extend from the surface to a depth of about 750 m, and the bathymetry-related patterns can extend from the seafloor to about 2,000 m above it. The larger reach of the bathymetry-related pattern is likely due to the weaker stratification in the deep ocean. The competition between surface and bottom controls of w_e in the ocean interior varies for different ocean regions, particularly in the Southern Ocean and out of the Southern Ocean. Figure 10 also shows the same calculation but for the Southern Ocean and other regions. In the Southern Ocean, the vertical velocity extends up to about 3,000 m above the bottom, but elsewhere, the bottom-related vertical velocity extends from the bottom up to about 800 m. Also, the surface-related velocity penetrates to different depths for the Southern Ocean and other regions as well. These clearly indicate the different dynamical regimes of vertical velocity in the global ocean, as well as the uniqueness of the Southern Ocean.

Two-dimensional views of the ocean circulation hide much important dynamics. The significant vertical variation of the spatial structure of w_e in the three-dimensional pictures (Figure 1) disappears in the zonally averaged views (Figure 5). In particular, in the Southern Ocean, zonal structures that appear related to the bathymetry disappear in the zonally averaged figures. These suppressed features, particularly the ones

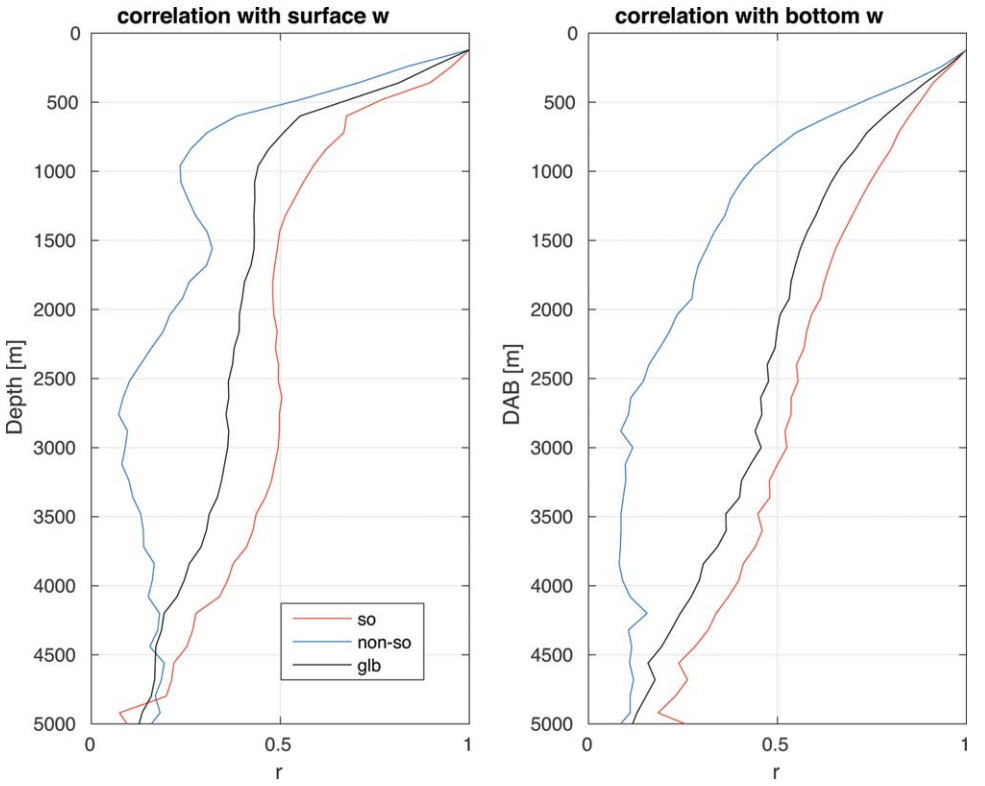

Figure 10. Correlation coefficients (r) between the 20 year means of the Eulerian vertical velocity at different depths. The left plot shows r between w_e at any depth and w_e near sea surface; the right plot shows r between w_e at any distance above the bottom (DAB) and w_e near the seafloor. If we arbitrarily choose $r = 0.5$ as a criterion, globally the wind-driven patterns can extend from the surface to the depth of about 750 m, and the bathymetry-related patterns can extend from the seafloor to about 2,000 m above it. Also, the Southern Ocean and the regions out of the Southern Ocean show clearly difference in the controls of w_e in the ocean interior.

related to the interaction of horizontal currents and topography, have important implications. Wind-driven upwelling in the Southern Ocean is often implicated in controls on atmospheric CO_2 and other properties (e.g., Anderson et al., 2009). State estimates show that a major portion of the vertical velocity in the deep ocean, particularly in the Southern Ocean, is in practice related to the strength of the deep ocean currents and bathymetry rather than directly wind-driven. Thus, in addition to the possible latitudinal wind shift (e.g., Toggweiler et al., 2006), changes in the wind stress intensity, which might lead to a changed Circumpolar Circulation, can induce changes in the deep ocean vertical velocity as well. As a consequence, more or less CO_2 can be transported into/out of the deep ocean due to wind intensity changes alone. This mechanism, through which the Southern Ocean can also regulate the atmospheric CO_2, is missed in the two-dimensional views of the ocean circulation.

The intensity of the global MOC is sometimes assumed equal to the deep and bottom water production rate, but the uncertainty of the existing estimates of the deep water production rate is large. Munk and Wunsch (1998) reviewed the then available estimates which ranged from 15 to 90 Sv. Integrals of the residual upwelling and downwelling in the present estimate show a global overturning of 70 Sv between about 1,000 and 3,000 m. This value is close to the upper-limit of the previous estimates (Stommel & Arons, 1960) and would include any entrained water in addition to that produced near the surface. Note that this value does not separate the upper and lower cells of the MOC, or separate components associated with different forcings (e.g., winds), so caution is advised in interpreting this value in the context of the MOC.

Estimates of the global vertical velocity permit insights into fundamental circulation physics. For example, consider the Eulerian vertical velocity, w_e in two classical ocean circulation theories. One is the Sverdrup relation, in which w_e in the deep ocean is assumed very weak and the integrated meridional transport can be related to the wind stress curl (e.g., Gill, 1982). Our estimate shows that even though this assumption is

reasonable in the subtropical basins, it is clearly not valid at high latitudes, particularly in the Southern Ocean. This finding is consistent with a few recent studies that directly evaluated Sverdrup Balance/Relation (e.g., Gray & Riser, 2014; Thomas et al., 2014; Wunsch, 2011). The appearance of complex spatial distributions of all forms of w precludes the general applicability of theories, such as Stommel-Arons, which assumed spatial uniformity. Understanding of the structure of the interior abyssal vertical velocity fields involves all of the elements determining the three-dimensional flow structure. Detailed studies focusing on interesting regions will be conducted in the future.

Acknowledgments
Data for this paper are available from ecco-group.org. Comments and suggestions from three anonymous reviewers help us greatly improve this paper. X.L. was grateful for the support from National Science Foundation through grant OCE-1736633. M.A.S. was supported by National Science Foundation grant OCE-1534618. C.W. was supported in part by National Science Foundation through grant OCE-0961713 and National Oceanic and Atmospheric Administration through grant NA10OAR4310135.

References

Adcroft, A., Hill, C., Campin, J. M., Marshall, J., & Heimbach, P. (2004). Overview of the formulation and numerics of the MIT GCM, In *Proceedings of the ECMWF Seminar on "Recent developments in numerical methods for atmospheric and ocean modelling"* (pp. 139–150). Reading, UK. Retrieved from https://www.ecmwf.int/en/learning/workshops-and-seminars/past-workshops/2004-annual-seminar

Aguiar, A., Cirano, M., Pereira, J., & Marta-Almeida, M. (2014). Upwelling processes along a western boundary current in the abrolhos-campos region of Brazil. *Continental Shelf Research*, *85*, 42–59.

Anderson, R. F., Ali, S., Bradtmiller, L. I., Nielsen, S., Fleisher, M. Q., Anderson, B. E., & Burckle, L. H. (2009). Wind-driven upwelling in the Southern Ocean and the deglacial rise in atmospheric CO_2. *Science*, *323*(5920), 1443–1448.

Balmaseda, M. A., Mogensen, K., & Weaver, A. T. (2013). Evaluation of the ECMWF ocean reanalysis system ORAS4. *Quarterly Journal of the Royal Meteorological Society*, *139*(674), 1132–1161.

Buckley, M. W., Ponte, R. M., Forget, G., & Heimbach, P. (2014). Low-frequency SST and upper-ocean heat content variability in the North Atlantic. *Journal of Climate*, *27*(13), 4996–5018.

Cummins, P. F., Masson, D., & Saenko, O. A. (2016). Vertical heat flux in the ocean: Estimates from observations and from a coupled general circulation model. *Journal of Geophysical Research: Oceans*, *121*, 3790–3802. https://doi.org/10.1002/2016JC011647

Danabasoglu, G., McWilliams, J. C., Gent, P. R. (1994). The role of mesoscale tracer transports in the global ocean circulation. *Science*, *264*(5162), 1123–1126.

de Boer, A. M., Graham, R. M., Thomas, M. D., & Kohfeld, K. E. (2013). The control of the Southern Hemisphere Westerlies on the position of the Subtropical Front. *Journal of Geophysical Research: Oceans*, *118*, 5669–5675. https://doi.org/10.1002/jgrc.20407

Dee, D. P., Uppala, S. M., Simmons, A. J., Berrisford, P., Poli, P., Kobayashi, S., . . . Vitart, F. (2011). The ERA-Interim reanalysis: configuration and performance of the data assimilation system. *Quarterly Journal of the Royal Meteorological Society*, *137*(656), 553–597.

Forget, G., Campin, J. M., Heimbach, P., Hill, C., Ponte, R. M., & Wunsch, C. (2015a). ECCO version 4: An integrated framework for non-linear inverse modeling and global ocean state estimation. *Geoscientific Model Development*, *8*(10), 3071–3104.

Forget, G., Ferreira, D., & Liang, X. (2015b). On the observability of turbulent transport rates by Argo: Supporting evidence from an inversion experiment. *Ocean Science*, *11*(5), 839–853.

Forget, G. L., & Ponte, R. M. (2015). The partition of regional sea level variability. *Progress in Oceanography*, *137*, 173–195.

Gent, P. R., & McWilliams, J. C. (1990). Isopycnal mixing in ocean circulation models. *Journal of Physical Oceanography*, *20*(1), 150–155.

Gill, A. E. (1982). *Atmosphere-ocean dynamics* (Vol. 30). San Diego, CA: Academic Press.

Gray, A. R., & Riser, S. (2014). A global analysis of Sverdrup balance using absolute geostrophic velocities from Argo. *Journal of Physical Oceanography*, *44*(4), 1213–1229.

Johnson, G. C., & Bryden, H. L. (1989). On the size of the Antarctic Circumpolar Current. *Deep Sea Research Part I: Oceanographic Research Papers*, *36*(1), 39–53.

Klein, P., Isern-Fontanet, J., Lapeyre, G., Roullet, G., Danioux, E., Chapron, B., . . . Sasaki, H. (2009). Diagnosis of vertical velocities in the upper ocean from high resolution sea surface height. *Geophysical Research Letters*, *36*, L12603. https://doi.org/10.1029/2009GL038359

Liang, X., Wunsch, C., Heimbach, P., & Forget, G. (2015). Vertical redistribution of oceanic heat content. *Journal of Climate*, *28*(9), 3821–3833.

Liang, X., & Yu, L. (2016). Variations of the global net air-sea heat flux during the "Hiatus" period (2001–10). *Journal of Climate*, *29*(10), 3647–3660.

Lu, Y., & Stammer, D. (2004). Vorticity balance in coarse-resolution global ocean simulations. *Journal of Physical Oceanography*, *34*(3), 605–622.

Marshall, D. (1995). Topographic steering of the Antarctic circumpolar current. *Journal of Physical Oceanography*, *25*(7), 1636–1650.

Marshall, J., & Radko, T. (2003). Residual-mean solutions for the Antarctic Circumpolar Current and its associated overturning circulation. *Journal of Physical Oceanography*, *33*(11), 2341–2354.

Marshall, J., & Speer, K. L. (2012). Closure of the meridional overturning circulation through Southern Ocean upwelling. *Nature Geoscience*, *5*(3), 171–180.

Munk, W. (1966). Abyssal recipes. *Deep Sea Research and Oceanographic Abstract*, *13*(4), 707–730.

Munk, W., & Wunsch, C. (1998). Abyssal recipes II: Energetics of tidal and wind mixing. *Deep Sea Research Part I: Oceanographic Research Papers*, *45*(12), 1977–2010.

Purkey, S. G., & Johnson, G. C. (2010). Warming of global abyssal and deep Southern Ocean Waters between the 1990s and 2000s: Contributions to global heat and sea level rise budgets. *Journal of Climate*, *23*(23), 6336–6351.

Qiao, L., & Weisberg, R. H. (1997). The zonal momentum balance of the equatorial undercurrent in the central pacific. *Journal of Physical Oceanography*, *27*(6), 1094–1119.

Qiu, B., & Huang, R. X. (1995). Ventilation of the North Atlantic and North Pacific: Subduction versus obduction. *Journal of Physical Oceanography*, *25*(10), 2374–2390.

Roughan, M., & Middleton, J. H. (2002). A comparison of observed upwelling mechanisms off the east coast of Australia. *Continental Shelf Research*, *22*(17), 2551–2572.

Schott, F., & Stommel, H. (1978). Beta spirals and absolute velocities in different oceans. *Deep Sea Research*, *25*(11), 961–1010.

Spall, M. A. (2003). Islands in zonal flow. *Journal of Physical Oceanography*, *33*(12), 2689–2701.

Spall, M. A., & Pickart, R. S. (2001). Where does dense water sink? A subpolar gyre example. *Journal of Physical Oceanography*, *31*(3), 810–826.

Speer, K. L., Rintoul, S. R., & Sloyan, B. (2000). The diabatic deacon cell. *Journal of Physical Oceanography*, *30*(12), 3212–3222.

Stammer, D., Balmaseda, M., Heimbach, P., Köhl, A., & Weaver, A. (2016). Ocean data assimilation in support of climate applications: Status and perspectives. *Annual Review of Marine Science*, *8*, (1), 491–518.

Stommel, H., & Arons, A. B. (1960). On the abyssal circulation of the world ocean. II: An idealized model of the circulation pattern and amplitude in oceanic basins. *Deep Sea Research*, *6*, 217–233.

Sverdrup, H. U. (1947). Wind-driven currents in a baroclinic ocean; with application to the equatorial currents of the eastern Pacific. *Proceedings of the National Academy of Sciences of the United States of America*, *33*(11), 318–326.

Talley, L. D. (2013). Closure of the global overturning circulation through the Indian, Pacific, and Southern Oceans: Schematics and transports. *Oceanography*, *26*(1), 80–97.

Thomas, M. D., De Boer, A. M., Johnson, H. L., & Stevens, D. P. (2014). Spatial and temporal scales of Sverdrup balance. *Journal of Physical Oceanography*, *44*(10), 2644–2660.

Toggweiler, J. R., Russell, J. L., & Carson, S. R. (2006). Midlatitude westerlies, atmospheric CO_2, and climate change during the ice ages. *Paleoceanography*, *21*, PA2005. https://doi.org/10.1029/2005PA001154

Wunsch, C. (2011). The decadal mean ocean circulation and Sverdrup balance. *Journal of Marine Research*, *69*(2), 417–434.

Wunsch, C., & Heimbach, P. (2013a). Dynamically and kinematically consistent global ocean circulation and ice state estimates. In S. Gerold, S. M. Griffies, J. Gould, & J. A. Church (Eds.), *Ocean circulation and climate: A 21st century perspective* (Vol. 103, pp. 553–579). Oxford, Amsterdam: Academic Press.

Wunsch, C., & Heimbach, P. (2013b). Two decades of the Atlantic meridional overturning circulation: Anatomy, variations, extremes, prediction, and overcoming its limitations. *Journal of Climate*, *26*(18), 7167–7186.

Wunsch, C., & Heimbach, P. (2014). Bidecadal thermal changes in the Abyssal Ocean. *Journal of Physical Oceanography*, *44*(8), 2013–2030.

Wyrtki, K. (1961). The thermohaline circulation in relation to the general circulation in the oceans. *Deep Sea Research*, *8*(1), 39–64.

Wyrtki, K. (1981). An estimate of equatorial upwelling in the Pacific. *Journal of Physical Oceanography*, *11*(9), 1205–1214.